IEEE Access
Multidisciplinary | Rapid Review | Open Access Journal

Received September 25, 2021, accepted October 11, 2021, date of publication October 18, 2021, date of current version October 26, 2021.

Digital Object Identifier 10.1109/ACCESS.2021.3121271

Performance Improvement of Multi-Rotor Axial Flux Vernier Permanent Magnet Machine by Permanent Magnet Shaping

IJAZ AHMAD[1], JUNAID IKRAM[1], MUHAMMAD YOUSUF[2], (Member, IEEE), RABIAH BADAR[1], SYED SABIR HUSSAIN BUKHARI[3], (Member, IEEE), AND JONGSUK RO[4,5]

[1]Department of Electrical and Computer Engineering, COMSATS University Islamabad, Islamabad 45550, Pakistan
[2]Department of Electrical and Computer Engineering, COMSATS University Islamabad, Abbottabad Campus, Abbottabad 22060, Pakistan
[3]Department of Electrical Engineering, Sukkur IBA University, Sukkur, Sindh 65200, Pakistan
[4]School of Electrical and Electronics Engineering, Chung-Ang University, Seoul 06974, South Korea
[5]Department of Intelligent Energy and Industry, Chung-Ang University, Seoul 06974, South Korea

Corresponding author: Jongsuk Ro (jongsukro@gmail.com)

This work was supported in part by the Brain Pool (BP) Program funded by the Ministry of Science and ICT through the National Research Foundation of Korea under Grant 2019H1D3A1A01102988, in part by the Basic Science Research Program through the National Research Foundation of Korea funded by the Ministry of Education under Grant 2016R1D1A1B01008058, and in part by the Human Resources Development of the Korea Institute of Energy Technology Evaluation and Planning (KETEP) funded by the Ministry of Trade, Industry and Energy, Korea Government under Grant 20204030200090.

ABSTRACT Permanent magnet vernier machines (PMVMs) are becoming progressively attentive because of their high efficiency and high torque density and can thus be utilized for direct-drive applications such as wind power and electric vehicles etc. This paper presents performance improvement of multi-rotor axial flux vernier permanent magnet (MR-AFVPM) machine with a proposed two-stage parallelogram-shaped PM. The proposed shaped PM reduces the cogging torque and torque ripples due to its skew effect. Furthermore, it also presents a comparative analysis of the conventional and proposed shape PM. Then 3D finite element analysis (FEA) is used for comparative analysis. Genetic algorithm (GA) associated with kriging method based on LHS is introduced and is used to optimize the proposed shaped PM for further performance improvement in terms of cogging torque, back EMFs, torque ripples, VTHD, output torque, flux density distributions, power factor and output power of the analyzed machines which are validated by 3D-FEA.

INDEX TERMS Axial flux, Vernier machine, torque density, cogging torque, genetic algorithm, 3D-FEA.

I. INTRODUCTION

Due to the large power flow related to electric machines, it is of significant importance to improve the efficiency of electrical machines for energy saving and environmental protection. In recent years, the environmental and energy problems are drawing more and more attention and many solutions have been proposed to address them. With the increase in energy demand and keeping in mind the environmental considerations, the research and design of highly efficient electric machines have received great attention. Gearless, direct-drive, low-speed machines become extra rewarding than high-speed machines with gearboxes, this is because of the previous machines that haven't any gearboxes and no associated problems *i.e.,* oil retention, noise problems, losses due to friction, etc. Though, conventional direct-drive machines are bulky and have low efficiency.

High torque density is the requirement for machines used in the direct drive system. Therefore, PM machines got too much attention due to high torque density [1]–[3]. PMVMs are magnetically geared machines that have a magnetic gearing effect due to flux modulation poles. The prier vernier reluctance machine is the base from which PMVMs are derived [4]. The high power features are achieved in the PMVM because of the magnetic gearing effect [5], [6]. Numerous pieces of literature determined that PMVMs show

The associate editor coordinating the review of this manuscript and approving it for publication was S. Ali Arefifar.

This work is licensed under a Creative Commons Attribution 4.0 License. For more information, see https://creativecommons.org/licenses/by/4.0/

several options to reduce the size and cost. The output power achieved in PMVMs is three times to equivalent of conventional PM machines for the similar volume and current [7]. However, PMVM is commonly designed for low-speed rotation due to large magnet pole numbers [8].

Various researchers have used the airgap field modulation to enhance the torque performances [9]–[11]. However, the PMVM is a typical simple structure machine having the features of an airgap modulation machine and high torque density. This machine has the great benefit of many working harmonics controlled by flux modulation poles rather than fundamental harmonics [10], [12]–[15]. The comparison of the permanent magnet synchronous machine (PMSM) and the permanent magnet vernier machine (PMVM) is summarized in Table 1 as reported in [16], [17].

TABLE 1. Comparison of the PMSMs and PMVMs.

Item	PMSMs	PMVMs
Torque density	Low	High
PM cost	High	Low
Efficiency	Low	High (at low speed)
Power factor	High	low

The PMVMs, which make use of magnetic gear effects to modify the magnetic fields, can produce high torque under comparatively low-speed operation [18], [19]. High torque density, structural compactness, and high efficiency make PMVMs machines more suitable for direct drive applications [20], [21].

Multi-objective optimization has got the most attraction recently and is used in the optimization of electric machines. To improve the average output torque of the switched reluctance motor, a multi-objective optimization analysis is investigated in [22]. In [23], another optimization technique based on particle swarm optimization (PSO) is discussed for cogging torque issue and efficiency enhancement of brushless DC motor. A 3D pareto front linear induction motor with finite element model evaluation is optimized and analyzed in [24]. This paper performs the well-known, simple, and practical optimization approach due to suitability with nonlinear data as implemented in [25].

The earlier research focuses mainly on the development of different axial flux topologies of the PMVMs machine. In this paper, the performance improvements of an MR-AFVPM machine are achieved by introducing a new two-stage parallelogram shape PM. The shape of the magnet is modified by proposing a new two steps parallelogram shape magnet from a basic trapezoidal shape magnet to improve the machine performance. In this paper, the structure and design parameters of a basic model of the MR-AFVPM machine were first reviewed. After that, a new magnet shape is proposed *i.e.,* two steps parallelogram, and the results are related to that of the basic model, and then the proposed model is optimized to further achieve the improvement in the machine performance.

II. MACHINE TOPOLOGY, DESIGN PROCEDURE, AND WORKING PRINCIPLE

The MR-AFVPM machine is comprised of three rotors and two stators as presented in Fig. 1. The magnets of the outer rotors are fixed on the rotor disc while the magnets of the inner rotor magnets are buried between the rotor cores making a spoke type structure.

The machine airgap flux density increases because of the spoke type inner rotor and thus greatly reduces its flux leakage [26]. The spoke-type assembly of the inner rotor is considered for the flux focusing effect, which efficiently increases the valuable flux and strengthens the flux lines that cross the two stators and rotor as a single loop and can increase the valuable flux in the core. The magnetism of the PMs and the rotor core can be utilized by adopting the spoke type assembly for the inner rotor [27]. The construction of the rotor also includes the determination of the magnet length and pole arc co-efficient. It is determined in [28], [29] that the pole arc co-efficient of a PM has a large effect on cogging torque.

In [30], it is presented that to minimize the leakage flux and to enhance the average value of the basic airgap flux density, both the two stators should have an offset of half slot pitch relative to each other. When there is a half slot pitch displacement between the two stators, the teeth are positioned as the generated magnetic flux in the rotor is passed through the stators with minimum magnetic reluctance, thereby increasing the basic airgap flux density. Drum-type winding is preferred to overcome the limitations of ring-type winding. The advantages of the drum-shaped winding, sometimes referred to as a toroidal stator winding, [31] are short end terminals, the simple stator core, and the simple construction. The manufacturing cost for the drum winding is reduced because fewer coils must be made here. The two stators are connected in series; hence, the total back EMF will be the sum of the two stators back EMF. The design specifications are given in Table 2.

The operating principle of MSPMVM is quite the same as the magnetically geared machines. The rotor and stator poles in the PMVM are correlated to the low and high pace rotors of magnetic gear. Stator tooth numbers in the PMVM are the same as the summation of winding pole pairs and rotor PM pole pairs which simplifies that the rotor PM pole pair numbers are more than the stator pole pair numbers. [32]–[34]. As a result, it violates the traditional approach of having the same rotor PM pole pair numbers and winding pole pairs. Although having an unequal number of pole pairs for rotor and stator, PMVM still achieved steady torque due to the flux modulation effect produced by stator teeth. A basic design principle for PMVM is explained as in (1).

$$Z_r = Z_s \pm p \tag{1}$$

where, Z_r, Z_s, and p represent the PM pole pair, slot number, and pole pair number of the stator winding. Particularly,

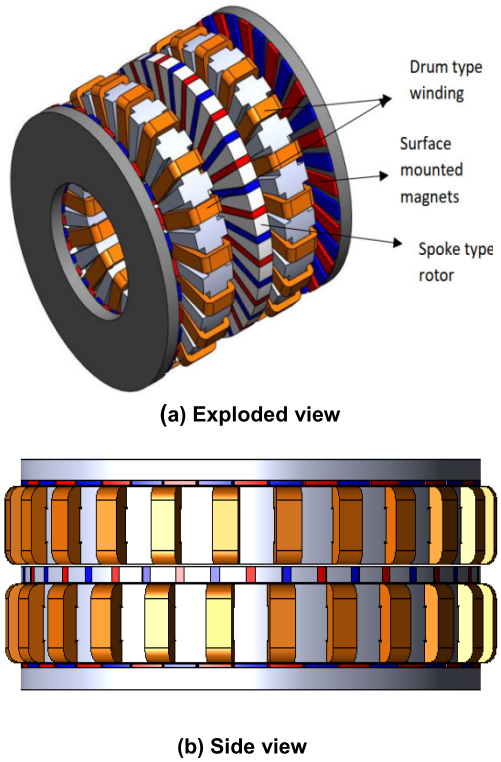

FIGURE 1. Configuration of the MR-AFVPM machine.

TABLE 2. Design parameters of machine.

Parameters	Unit	Values
Power	kW	8
Rated Speed	rpm	320
Winding pole pairs	-	1
Stator tooth numbers	-	18
Rotor outer diameter	mm	254
Rotor inner diameter	mm	152
Axial length	mm	128.8
Airgap length	mm	1
PM thickness of inner rotor	mm	7
Magnet (N40UH)	T	B_r =1.23
PM thickness of outer router	mm	4

the essential low-speed high torque feature of PMVM is achieved by the magnetic gearing effect, hence, minimum movement of rotor leads to larger flux variations [35]. It's normal practice in the design process to make Zr larger than p. When flux got a rotation of 360 degrees, the rotation achieved by the rotor is only $360/Z_r$ as described in (2).

$$\frac{\omega_r}{\omega_{MMF}} = \frac{Rotor\ speed}{Rotating\ Field\ Speed} = \frac{\tau_r}{\tau_{MMF}} = \frac{p}{Z_r} \tag{2}$$

where ω_r, ω_{MMF}, T_r, and T_{MMF} represent the rotor speed, flux speed, rotor slot pitch, and MMF pole pitch. The flux focusing effect is quite the same as briefly described in [36].

The mathematical discussion of the basic model is briefly discussed here is the same as discussed in [37]. The input power calculations can be made as discussed in (3).

$$P_{in} = 2\frac{m}{T}\int_0^T E_m \sin(\omega t) I_m \sin(\omega t) dt \tag{3}$$

where m, E_m, and I_m represents the phase numbers, the amplitude of back EMF, and the phase current while the output power calculations are depicted in (2) where γ is for efficiency in (4).

$$P_{out} = \gamma m E_m I_m \tag{4}$$

The flux can be computed as in (5)

$$\varphi = \varphi_m \cos(N_p \alpha_r) \tag{5}$$

where φ denotes the magnitude of flux, α_r shows the rotor position and N_p represents the numbers of rotor poles, respectively. The back EMF can be expressed as in (6).

$$e(t) = N_{ph}\omega_r N_P \varphi_m \sin(N_p \alpha_r) \tag{6}$$

where N_{ph} and ω_r show the phase coil turns and angular speed of the rotor, respectively. By putting (3) in (4), back EMF is determined as in (7).

$$e(t) = N_{ph}\omega_r N_P k_d k_f B_g \alpha_i \frac{1}{N_s}\frac{\pi}{4}(D_{out}^2 - D_{in}^2) \tag{7}$$

where, k_d, B_g,N_s, D_{out}, and D_{in} represent the airgap flux density coefficient, lux leakage coefficient, air-gap flux density, slot numbers, pole arc coefficient, the outer and inner diameter of the rotor, respectively. The armature current is computed as in (8).

$$I_m = \frac{\sqrt{2} A_e \pi D_{in}}{2 m N_{ph}} \tag{8}$$

where Ae shows the electrical loading. By putting the (5), (6) in (2) gives the input power as given in (9).

$$P_{in} = \frac{\sqrt{2\pi^3}}{240}\frac{N_p}{N_s} k_d k_f k_{io}(1 - k_{io}^2) A_e B_g \alpha_i D_{out}^3 n_{rpm} \gamma \tag{9}$$

where k_{io} represents the ratio of inner and outer diameters and n_{rpm} represents the rotor speed, respectively. Furthermore, the output torque can be computed as in (10).

$$T_{out} = \frac{\sqrt{2}}{240}\pi^2 \frac{N_P}{N_s} k_d k_f k_{io}(1 - k_{io}^2) A_e B_g \alpha_i D_{out}^3 \gamma \tag{10}$$

It is very clear from (9) and (10), the power and torque are dependent on the A_e, B_g, and N_p/N_s. From (9), the outer diameter can be represented as in (11).

$$D_{out} = \sqrt[3]{\frac{240 P_{out} N_s}{\sqrt{2}\pi^3 N_r k_d k_f k_{io}(1-k_{io}^2) A_e B_g \alpha_i n_{rpm} \gamma}} \quad (11)$$

Flux density distribution is illustrated in Fig. 3 that describes the maximum flux density of 2.00T is achieved and there is no saturation observed for the MR-AFVPM machine. MR-AFVPM machine with Spoke arranged PM achieved a greater airgap flux density as given in Fig. 4, which verifies the flux focusing effect. The fast Fourier transform (FFT) of each harmonic of the airgap flux density is given in Fig. 5, where the fundamental harmonic component is at the magnetic pole pair number $Z_r = 17$, the 35^{th} is the working harmonic with one rotor pole pair number.

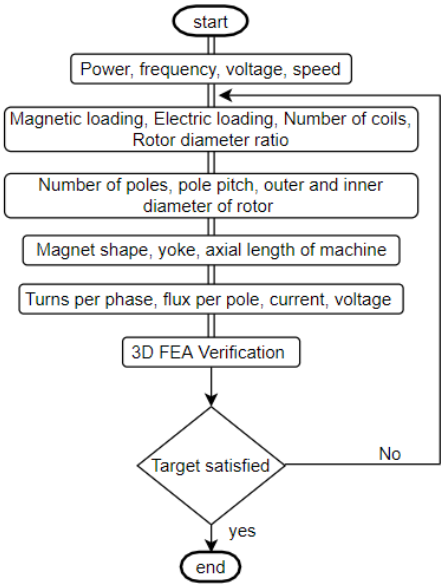

FIGURE 2. Design process.

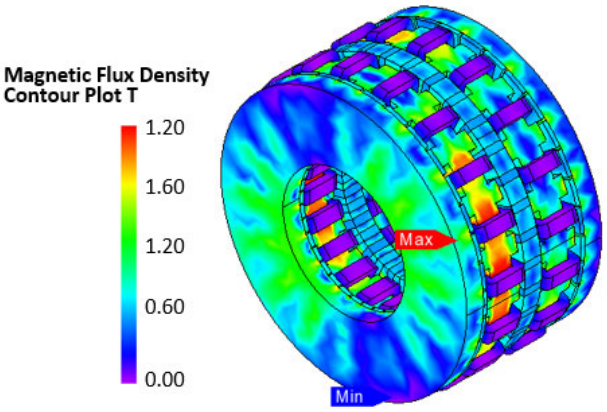

FIGURE 3. Flux density distribution of initial design.

III. PROPROSED MAGNET SHAPE

Cogging torque is caused by the attraction of magnets with the stator slots. To be specific, it occurs due to the attraction

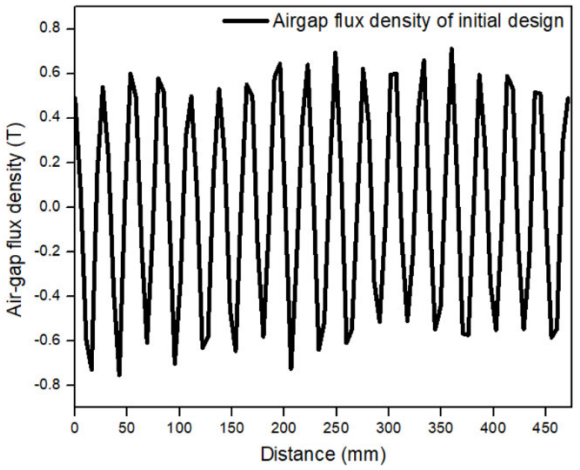

FIGURE 4. Airgap flux density.

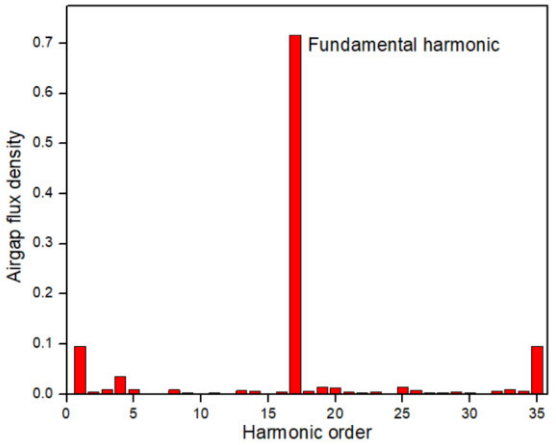

FIGURE 5. Harmonic spectra of airgap flux density.

of the magnetic flux with stator reluctance variations initiated by the stator slots.

$$T_{cog} = -\frac{1}{2}\theta_g^2 \frac{dR}{d\theta} \quad (12)$$

The magnetic flux passing through each airgap is presented by θ_g while R shows the stator reluctance. In (12), it is shown that to decrease the cogging torque either magnetic flux or reluctance variation must be reduced. Conversely, a reduction in magnetic flux deteriorates the machine performance and hence, it is not considered a possible solution to decrease the cogging torque. Therefore, reducing reluctance variation is considered a useful method to decreases the cogging effect. Skewing magnets or modifying the shape of magnets contribute somewhat to decrease this deviation and thus decrease the cogging torque. The physical geometry and the magnet pole-arc of the magnet will determine the maximum value and profile of cogging torque. Decreasing the magnet pole arc ratio decreases leakage of the magnet, but also decreases the magnetic flux and thus the output torque. Consequently,

a settlement is commonly required throughout the design of the rotor.

In [38], a triple-rotor axial-flux vernier permanent magnet machine is investigated to explain the initial machine principle with some initial analysis. The performance of the axial flux PM magnet motors is investigated in [39] by considering the various PM shapes. The concept used in the proposed permanent magnet shaping is close to the step skewing method. However, this skewing concept is introduced, in this paper, for the proposed PMVM topology to analyze its output performances, furthermore, the optimization algorithm based on the krigging method associated with the Latin Hypercube Sampling (LHS) and the genetic algorithm (GA) is implemented to find the magnet shape.

In this paper, a new two-stage parallelogram shape magnet is considered for the performance improvement of the analyzed machine. The comparison of both the basic trapezoidal shape magnet and two-stage parallelogram shape magnet is shown in Fig. 6. In Fig. 6 it is shown that the trapezoidal shape magnet aligned with the maximum amount of stator teeth while also in Fig.6 the two steps parallelogram shape magnet aligned with less amount of stator teeth. Now according to the definition of cogging torque, there will be less attractive in the case of two steps parallelogram shape magnet and the stator teeth, hence the cogging torque will be small. Magnet skewing is an active and modest technique for minimizing the cogging torque commonly employed in PM machines. The skew angle is given in (13).

$$\theta_{skew} = \frac{2\pi}{N_s} \tag{13}$$

where N_s and θ_{skew} show the stator slot numbers and skew angle. Because of the difference in inner and outer radius, the skew angle is generally narrow but not the same. Though, this angle is greater in AFPM machines because the inner and outer diameters of the magnets differ. However, it can be easily used in AFPM machines because of its simpler magnet geometry and flat magnet surface than in RFPM machines. Even though the skewing rotor is a renowned technique to decrease the cogging torque in PM machines [22] but it is not common practice because of implementation difficulties. Though, a modified form known as stepped rotor magnets [28], is more common because the implementation can be made simpler.

The angle of one cogging torque cycle should be chosen as the skew angle because of the leading harmonic factor of the cogging torque, this means $\theta_{skew} = 360°/18 = 20°$ in mechanical. Thus, by using the two steps the skew angle for each step is $\theta_{skew\_step} = \theta_{skew}/2 = 10°$. A comparison is carried out between the basic trapezoidal shape magnet and the two-step skew magnet in the next section.

IV. FEA-BASED PERFORMANCE ANALYSIS

The results of the conventional trapezoidal and the two-stage parallelogram shape magnet from 3D FEA are shown in this section. The conventional trapezoidal shape magnet has large

a) Conventional magnet shape b) Proposed magnet shape

FIGURE 6. Illustration of conventional and proposed magnet shapes.

cogging torque at the expense of a slight decrease in back EMF as related to the proposed shape magnet.

The comparison between the basic model back EMF and the proposed model back EMF is shown in Fig. 7. The basic model shows the back EMF of 112.2 V_{rms} and that of the proposed model is 113.84 V_{rms}. Therefore, the percentage decrease resulted in back EMFs because of the proposed shaped PM is 1.46%. The decrease in back EMFs is because of the decrease in the flux density with the proposed shaped PM.

The cogging torque comparison of the basic and proposed designs is represented in Fig. 8. The conventional model peak to peak cogging torque is 16.8 Nm and that of the proposed design is 11.7 Nm. Thus, a percentage reduction of 30.35% in cogging torque is attained with the proposed shaped model. Thus, with the proposed shape magnet, there is less amount of attraction between the PM and the stator tooth. The less attraction is due to the asymmetrical arrangement of magnets on the rotor disc.

The average torque of both the basic and the proposed design is shown in Fig. 9. The average output torque of the proposed model is 193.509 Nm, and it is 183.092 Nm for the base model. Thus, the percentage improvement in average torque is 5.6894% with the proposed shaped model. Furthermore, the proposed design shows 6.26% torque ripples while the basic model has 8.88% torque ripples. Therefore, the percentage reduction of the torque ripples with the proposed model is 29.54%.

The output power comparison of the basic and proposed model is depicted in Fig. 10. The average output power of the conventional model is 8.4 kW and that of the conventional model is 8 kW. This exhibits that the proposed model has enhanced output power when compared with conventional design and the percentage increase of the average output torque is 5%. The quantitative comparison of both models is presented in Table 3.

The cogging torque reduction is 30.7% and that of the back EMF is 1.46%. The percentage improvement of the average output torque, torque ripples, and power are 5.68%, 29.54%, and 5%. As can be seen, significant cogging torque reduction is achieved in the proposed model. However, back EMF also reduces with the proposed model, but this reduction

is very slight as compared to the cogging torque reduction. Furthermore, the improvement in torque and power is also obtained with the proposed model. In addition, a significant reduction in torque ripples is also achieved with the proposed model.

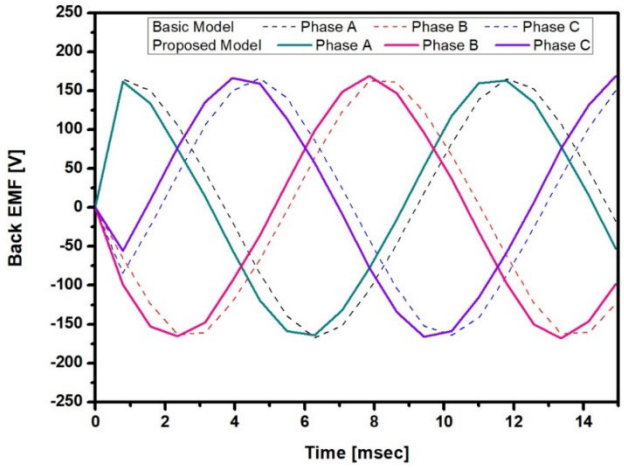

FIGURE 7. Back EMF comparison.

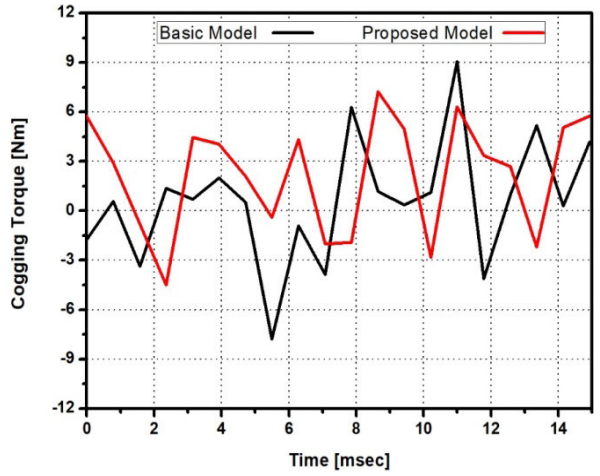

FIGURE 8. Cogging torque comparison.

V. OPTIMIZATION PROCESS

The above-discussed PMVM was developed only by placing a proposed shape PMs to the slot of the rotor. This leads not only to enhance the average output torque but also to a decrease in the torque ripples. By optimization of the proposed magnet shape, it is more convenient that the torque ripple and the average output torque can become better. Therefore, an efficient optimization technique is applied that combines the kriging method and genetic algorithm (GA) [40] to optimize the rotor shape, and hence, average torque and torque ripple are improved with fixed motor size without compromising the efficiency.

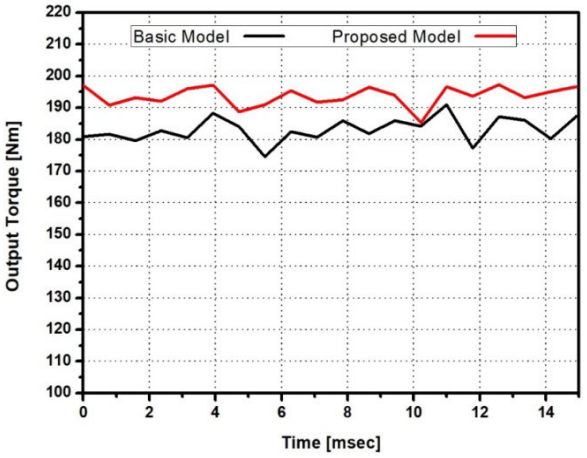

FIGURE 9. Output torque comparison.

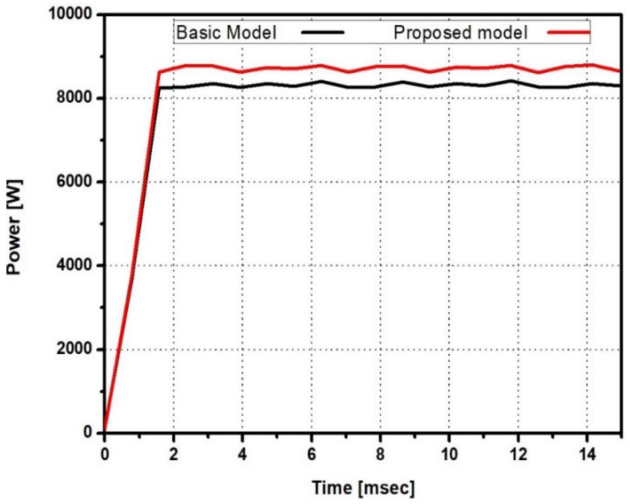

FIGURE 10. Output power comparison.

TABLE 3. Quantitative analysis of basic and proposed model.

Parameters	Basic Model	Proposed Model
Back emf	112.2 V_{rms}	113.8 V_{rms}
Cogging Torque	16.8 Nm	11.7 Nm
Average Output Torque	183.092 Nm	193.509 Nm
Torque Ripple	8.88%	6.26%
Power factor	0.87	0.85
Power	8 kW	8.4 kW

As per the design specifications of the motor, the objective functions, constraints, and design variables are preserved. The two design variables are to be changed for the rotor as

shown in Fig. 11. The flow of the final design procedure is illustrated in Fig. 12. The Latin hypercube sampling (LHS) is applied for searching the testing points in the computational domain of design variables X_1, X_2. By applying the LHS that matches certain design variables, the sample values are randomly and evenly spaced across all areas. The model came up with 2D FEA analysis creates results by performing the kriging method in the PIAnO software by PIDOTEC Inc. [41]. After that, the GA evaluates the suitability of a modeling function generated by the kriging model; the optimal results are thus found by the population. The fitness modeling function $F(i)$ performed in GA is presented in (8) as in [33]. by PIDOTEC Inc. [39]. After that, the Generic Algorithm evaluates the suitability of a modeling function generated by the kriging model; the optimal results are thus found by the population. The fitness modeling function $F(i)$ performed in GA is presented in (8) as in [40].

$$F(i) = f(i) + P(i) \tag{14}$$

where $f(i)$ shows the multi-objective function, $P(i)$ depicts the penalty function and i represents the vector of the design variables. Finally, FEA tested the design results achieved in optimization. If the FEA results did not meet the requirement of the target, the range of design variables is considered again, and the procedure is repeated until they are met. Design variables, objective functions, and constraints are described below as in (15), (16), and (17), respectively.

$$\begin{aligned} &X_1 \rightarrow Length\ of\ magnet[31mm - 35mm] \\ &X_2 \rightarrow Width\ of\ magnet[8mm - 12mm] \end{aligned} \tag{15}$$

$$Minimizing\ cogging\ torque \\ Maximizing\ back\ EMF \tag{16}$$

$$Cogging\ torque < 11.7Nm \\ EMF > 113.8V_{rms} \tag{17}$$

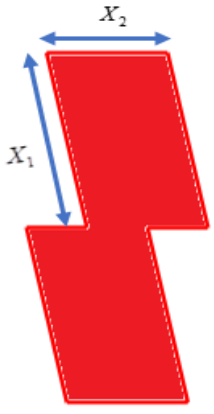

FIGURE 11. Design variables.

VI. PERFORMANCE COMPARISON OF PROPOSED AND OPTIMIZED MODELS

After the optimization of the proposed magnet shape, a new model is designed based on optimal values and is analyzed by using 3D-FEA. This section presents the analysis comparison of the optimized and proposed and models.

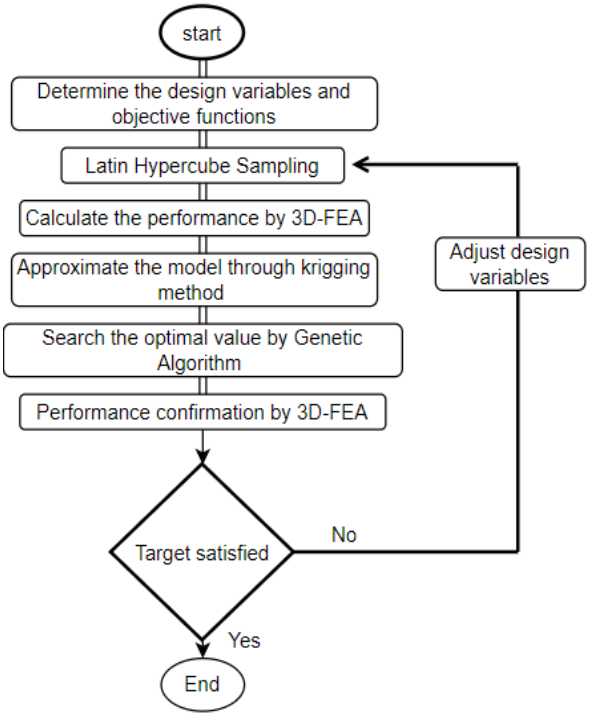

FIGURE 12. Optimization process.

The back EMF comparison of the proposed and optimized model is given in Fig. 13, the optimized model back EMF is better than the proposed model. The back EMF achieved in the proposed model is 113.8 V_{rms} and it is 118.7 V_{rms} for the optimized model. Thus, a percentage enhancement in the back EMF of the optimized model is 4.30%.

Cogging torque of the optimized and proposed machines is presented in Fig. 14. The quantitative analysis of cogging torque shows that the cogging torque of the optimal machine is reduced to 11.3 Nm from 11.7 Nm. Thus, a percentage decrease of 3.53% is obtained due to the optimization of the proposed model.

The average output torque of both the machine models is presented in Fig. 15. The output torque of the optimal machine is more than the proposed machine. The average output torque of the optimized model is 200.6 Nm, and the proposed model torque was 193.509 Nm. This resulted in a 3.5349% improvement in the average output torque due to optimization.

The output power of both designs is given in Fig. 16. The average output power of the optimized design is 8.45 kW and that of the proposed model is 8.4 kW. This exhibits the more output power is achieved in the optimized design.

The quantitative analysis of both models is given in Table 4. As it is clearly seen from Table 4, the performance of the proposed machine is improved in the optimized machine due to a suitable optimization process. The percentage reduction in

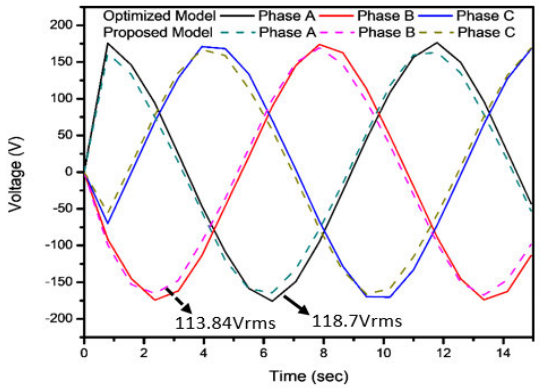

FIGURE 13. Back EMF comparison.

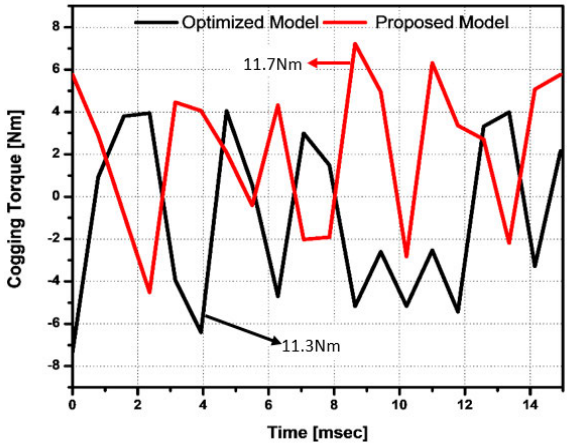

FIGURE 14. Cogging torque comparison.

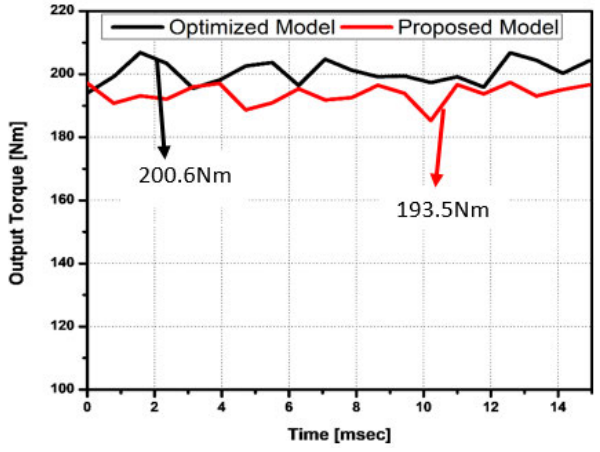

FIGURE 15. Output torque comparison.

cogging torque is 3.5398% and the percentage enhancement in the average output torque is 3.5349%.

MR-AFVPM machine topology applies flux focusing effect which can increase the airgap flux density and magnet flux utilization as explained in [36]. Hence, fewer ampere-turns are desired for required output power. So, reduced winding reactance is achieved which can improve the power factor of this topology. Also, this topology discourages leakage flux between adjacent PMs. The power factor is also considered for machine models and improved as described in Table 4.

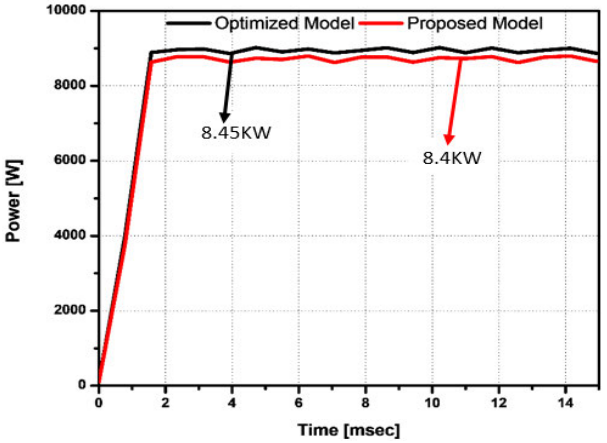

FIGURE 16. Output power comparison.

TABLE 4. Quantitative analysis of proposed and optimized model.

Parameters	Proposed Model	Optimized Model
Back emf	113.8 V_{rms}	118.7 V_{rms}
Cogging Torque	11.7 Nm	11.3 Nm
Average Output Torque	193.509 Nm	200.6 Nm
Power factor	0.85	0.88
Power	8.4 kW	8.45 kW

VII. CONCLUSION

The MR-AFVPM machine topology is adopted in the design with four airgaps sharing the same rotor for more torque production and reasonable space utilization. The spoke-type structure of the inner rotor is developed for the flux focusing effect, which can efficiently increase the corresponding flux while forcing the flux lines to cross throughout the entire machine as compared to the other two separate torque components as in the case of a normal dual-stator PM machine. Reducing the reluctance in the main flux path and making a new path for main flux, for this purpose the two stators are shifted by an angle to minimize the flux leakage. Due to the symmetrical and multi-stack design, the machine has a better fault-tolerant capability. A new two stages parallelogram shape magnet is proposed, and the reduction achieved in PM volume is 13% as compared to the conventional shape magnet while the improvement in performance is not compromised.

The optimization of the proposed shape is carried out to achieve the better performance of the analyzed machine in terms of back EMF, cogging torque, average output torque, power factor, and output power. The 30.35% reduction in the cogging torque is achieved due to the proposed PM shape and 3.41% further reduction is attained in the optimization process. The average output torque enhancement is 9.56% in the final optimized model as compared to the initial model. The power factor is improved to 0.88 in the optimized model. The comparison of the analyzed multi-rotor AFVPM machine consists of various topology *i.e.*, single-sided, and double-sided AFVPM machines, with the analytical and experimental validation are to be considered for future work.

REFERENCES

[1] Q. Chen, G. Xu, G. Liu, W. Zhao, Z. Lin, and L. Liu, "Torque ripple reduction in five-phase IPM motors by lowering interactional MMF," *IEEE Trans. Ind. Electron.*, vol. 65, no. 11, pp. 8520–8531, Nov. 2018.
[2] Y. Feng, F. Li, S. Huang, and N. Yang, "Variable-flux outer-rotor permanent magnet synchronous motor for in-wheel direct-drive applications," *Chin. J. Elect. Eng.*, vol. 4, no. 1, pp. 28–35, Mar. 2018.
[3] L. Xu, W. Zhao, G. Liu, J. Ji, and S. Niu, "A novel dual-permanent-magnet-excited machine with non-uniformly distributed permanent-magnets and flux modulation poles on the stator," *IEEE Trans. Veh. Technol.*, vol. 69, no. 7, pp. 7104–7115, Jul. 2020.
[4] C. H. Lee, "Vernier motor and its design," *IEEE Trans. Power App. Syst.*, vol. 82, no. 66, pp. 343–349, Jun. 1963.
[5] D. Jang and J. Chang, "Performance comparison of PM synchronous and PM Vernier machines based on equal output power per unit volume," *J. Elect. Eng. Technol.*, vol. 11, no. 1, pp. 150–156, 2016, doi: 10.5370/jeet.2016.11.1.150.
[6] F. Wu and A. M. El-Refaie, "Permanent magnet Vernier machines: A review," in *Proc. XIII Int. Conf. Electr. Mach. (ICEM)*, Sep. 2018, pp. 372–378.
[7] B. Kim and T. A. Lipo, "Operation and design principles of a PM Vernier motor," *IEEE Trans. Ind. Appl.*, vol. 50, no. 6, pp. 3656–3663, Nov. 2014.
[8] F. Zhao, T. A. Lipo, and B.-I. Kwon, "Dual-stator interior permanent magnet Vernier machine having torque density and power factor improvement," *Electr. Power Compon. Syst.*, vol. 42, no. 15, pp. 1717–1726, 2014, doi: 10.1080/15325008.2014.950360.
[9] M. Cheng, P. Han, and W. Hua, "General airgap field modulation theory for electrical machines," *IEEE Trans. Ind. Electron.*, vol. 64, no. 8, pp. 6063–6074, Aug. 2017.
[10] Z. Q. Zhu and Y. Liu, "Analysis of air-gap field modulation and magnetic gearing effect in fractional-slot concentrated-winding permanent-magnet synchronous machines," *IEEE Trans. Ind. Electron.*, vol. 65, no. 5, pp. 3688–3698, May 2018.
[11] Y. Wang, W. Xu, X. Zhang, and W. Ma, "Harmonic analysis of air gap magnetic field in flux-modulation double-stator electrical-excitation synchronous machine," *IEEE Trans. Ind. Electron.*, vol. 67, no. 7, pp. 5302–5312, Jul. 2020.
[12] P. Su, W. Hua, Z. Wu, Z. Chen, G. Zhang, and M. Cheng, "Comprehensive comparison of rotor permanent magnet and stator permanent magnet flux-switching machines," *IEEE Trans. Ind. Electron.*, vol. 66, no. 8, pp. 5862–5871, Aug. 2019.
[13] L. Xu, G. Liu, W. Zhao, X. Yang, and R. Cheng, "Hybrid stator design of fault-tolerant permanent-magnet Vernier machines for direct-drive applications," *IEEE Trans. Ind. Electron.*, vol. 64, no. 1, pp. 179–190, Jan. 2017.
[14] W. Zhao, K. Du, and L. Xu, "Design considerations of fault-tolerant permanent magnet Vernier machine," *IEEE Trans. Ind. Electron.*, vol. 67, no. 9, pp. 7290–7300, Sep. 2020.
[15] X. Ren, D. Li, R. Qu, Z. Yu, and Y. Gao, "Investigation of spoke array permanent magnet Vernier machine with alternate flux bridges," *IEEE Trans. Energy Convers.*, vol. 33, no. 4, pp. 2112–2121, Dec. 2018.
[16] P. M. Tlali, R.-J. Wang, and S. Gerber, "Comparison of PM Vernier and conventional synchronous 15 kW wind generators," in *Proc. XIII Int. Conf. Electr. Mach. (ICEM)*, Sep. 2018, pp. 2065–2071.
[17] P. M. Tlali, R.-J. Wang, S. Gerber, C. D. Botha, and M. J. Kamper, "Design and performance comparison of Vernier and conventional PM synchronous wind generators," *IEEE Trans. Ind. Appl.*, vol. 56, no. 3, pp. 2570–2579, May 2020.
[18] E. Spooner and L. Hardock, "Vernier hybrid machines," *IEE Proc.-Electr. Power Appl.*, vol. 150, no. 6, pp. 655–662, Nov. 2003.
[19] A. Toba and T. A. Lipo, "Generic torque-maximizing design methodology of surface permanent-magnet Vernier machine," *IEEE Trans. Ind. Appl.*, vol. 36, no. 6, pp. 1539–1546, Nov. 2000.
[20] S. Niu, S. L. Ho, W. N. Fu, and L. L. Wang, "Quantitative comparison of novel Vernier permanent magnet machines," *IEEE Trans. Magn.*, vol. 46, no. 6, pp. 2032–2035, Jun. 2010.
[21] D. Li, R. Qu, and T. A. Lipo, "High-power-factor Vernier permanent-magnet machines," *IEEE Trans. Ind. Appl.*, vol. 50, no. 6, pp. 3664–3674, Dec. 2014.
[22] L. Lebensztajn, C. A. R. Marretto, and F. A. B. Perdiz, "A multi-objective analysis of a special switched reluctance motor," *COMPEL-Int. J. Comput. Math. Elect. Electron. Eng.*, vol. 24, no. 3, pp. 931–941, 2005.
[23] U. Nagalingam, B. Mahadevan, K. Vijayarajan, and A. P. Loganathan, "Design optimization for cogging torque mitigation in brushless DC motor using multi-objective particle swarm optimization algorithm," *COMPEL-Int. J. Comput. Math. Electr. Electron. Eng.*, vol. 34, no. 4, pp. 1302–1318, Jul. 2015.
[24] J. Gong, A. Claudiu Berbecea, F. Gillon, and P. Brochet, "Multi-objective optimization of a linear induction motor using 3D FEM," *COMPEL-Int. J. Comput. Math. Elect. Electron. Eng.*, vol. 31, no. 3, pp. 958–971, 2012.
[25] F. Zhao, T. A. Lipo, and B. Kwon, "Magnet flux focusing design of double stator permanent magnet Vernier machine," in *Proc. COMPUMAG*, Jul. 2013.
[26] T. Li and G. Slemon, "Reduction of cogging torque in permanent magnet motors," *IEEE Trans. Magn.*, vol. 24, no. 6, pp. 2901–2903, Nov. 1988.
[27] T. Ishikawa and G. R. Slemon, "A method of reducing ripple torque in permanent magnet motors without skewing," *IEEE Trans. Mag.*, vol. 29, no. 2, pp. 2028–2031, Mar. 1993.
[28] Y. Lu, J. Li, H. Lu, R. Qu, L. Xiao, D. Li, and R. Zhang, "Six-phase double-stator inner-rotor axial flux PM machines with novel detached winding," *IEEE Trans. Ind. Appl.*, vol. 53, no. 3, pp. 1931–1941, Jun. 2017.
[29] B. J. Chalmers, E. Spooner, O. Honorati, F. Crescimbini, and F. Caricch, "Compact permanent-magnet machines," *Electr. Mach. Power Syst.*, vol. 25, no. 6, pp. 635–648, 1997.
[30] D. Hanselman, *Brushless Permanent-Magnet Motor Design*. New York, NY, USA: McGraw-Hill, 1994.
[31] R. Qu, D. Li, and J. Wang, "Relationship between magnetic gears and Vernier machines," in *Proc. Int. Conf. Electr. Mach. Syst.*, Beijing, China, Aug. 2011, pp. 1–6.
[32] K. Atallah and D. Howe, "A novel high-performance magnetic gear," *IEEE Trans. Magn.*, vol. 37, no. 4, pp. 2844–2846, Jul. 2001.
[33] L. Jian, K. T. Chau, and J. Z. Jiang, "A magnetic-geared outer-rotor permanent-magnet brushless machine for wind power generation," *IEEE Trans. on Ind. Appl.*, vol. 45, no. 3, pp. 954–962, May/Jun. 2009.
[34] M. Takano and S. Shimomura, "Improvement of torque density of variable reluctance Vernier machine for hybrid electric vehicle," in *Proc. IEEE Energy Convers. Congr. Expo.*, Denver, CO, USA, Sep. 2013, pp. 1205–1212.
[35] D. Fukai and S. Shimomura, "Integrated radial and dual axial-flux variable-reluctance Vernier machine," in *Proc. 40th Annu. Conf. IEEE Ind. Electron. Soc. (IECON)*, Dallas, TX, USA, Oct. 2014, pp. 682–688.
[36] F. Zhao, T. A. Lipo, and B. I. Kwon, "A novel dual-stator axial-flux spoke-type permanent magnet Vernier machine for direct-drive applications," *IEEE Trans. Magn.*, vol. 50, no. 11, pp. 1–4, Nov. 2014.
[37] M. Bilal, J. Ikram, A. Fida, S. S. H. Bukhari, N. Haider, and J. Ro, "Performance improvement of dual stator axial flux spoke type permanent magnet Vernier machine," *IEEE Access*, vol. 9, pp. 64179–64188, 2021.
[38] R. Zhang, J. Li, R. Hai, Q. Da, and W. Li, "A novel triple-rotor axial-flux Vernier permanent magnet machine," in *Proc. IEEE Int. Conf. Appl. Supercond. Electromagn. Devices (ASEMD)*, Nov. 2015, pp. 537–538.
[39] E. Cetin and F. Daldaban, "Analyzing the profile effects of the various magnet shapes in axial flux PM motors by means of 3D-FEA," *Electronics*, vol. 7, no. 2, p. 13, Jan. 2018.
[40] M. Yousuf, F. Khan, J. Ikram, R. Badar, S. S. H. Bukhari, and J. Ro, "Reduction of torque ripples in multi-stack slotless axial flux machine by using right angled trapezoidal permanent magnet," *IEEE Access*, vol. 9, pp. 22760–22773, 2021.
[41] *PIAnO Introduction*. Accessed: Apr. 1, 2018. [Online]. Available: http://pidotech.com/en/product/piano.aspx

IJAZ AHMAD received the B.S. degree in electrical power engineering from COMSATS University Islamabad, Abbottabad Campus, Abbottabad, Pakistan, in 2016, and the M.S. degree in electrical engineering from COMSATS University Islamabad, Islamabad, Pakistan, in 2019. His research interests include design, analysis and optimization of permanent magnet Vernier machines, and axial flux permanent magnet machines.

JUNAID IKRAM received the B.E. degree in electrical engineering from the University of Engineering and Technology, Lahore, Pakistan, in 2005, the M.S. degree from Hanyang University, South Korea, in 2009, and the Ph.D. degree in electrical engineering from COMSATS University Islamabad, Pakistan, in 2017. Currently, he is working as a Senior Engineer with COMSATS University Islamabad. His research interests include design, analysis and optimization of axial flux machines, Vernier machines, wound rotor synchronous machine, hybrid flux switching machines, and modeling of the machine losses.

MUHAMMAD YOUSUF (Member, IEEE) received the B.S. degree in electrical engineering (electronics) from the Federal Urdu University of Arts Science & Technology (FUUAST), Islamabad, Pakistan, in 2015, and the M.S. degree in electrical engineering from COMSATS University Islamabad, Islamabad, in 2019. He is currently pursuing the Ph.D. degree in electrical engineering with COMSATS University Islamabad, Abbottabad Campus, Abbottabad, Pakistan. His research interests include design, analysis and optimization of permanent magnet flux switching machines, linear flux switching machines, and axial flux permanent magnet machines.

RABIAH BADAR received the M.S. degree in computer engineering and the Ph.D. degree in electrical engineering from COMSATS University Islamabad, in 2007 and 2009, respectively. From February 2015 to May 2015, she was with Namal Institute, Mianwali, Pakistan, as an Assistant Professor. After that, she joined COMSATS University Islamabad as an Assistant Professor. She served as a pioneer in charge of the B.S. Electrical (Power) Engineering Program. She is the author of many international, peer-reviewed journal research articles, conference papers, and book chapters. She has successfully supervised many undergraduate and graduate research thesis. Her research interests include artificial intelligence, optimization, soft computing, power system stability and control, nonlinear adaptive control, FACTS, HVDC, and renewable energy systems.

SYED SABIR HUSSAIN BUKHARI (Member, IEEE) received the B.E. degree in electrical engineering from the Mehran University of Engineering & Technology Jamshoro, Pakistan, in 2009, and the Ph.D. degree from the Department of Electronic Systems Engineering, Hanyang University, South Korea, in 2017. He joined Sukkur IBA University as an Assistant Professor, in December 2016. He is currently working as a Research Professor with Chung-Ang University, Seoul, South Korea, under the Korean Research Fellowship (KRF) Program. His main research interests include electric machine design, power quality, and drive controls.

JONGSUK RO received the B.S. degree in mechanical engineering from Hanyang University, Seoul, South Korea, in 2001, and the Ph.D. degree in electrical engineering from Seoul National University (SNU), Seoul, in 2008. He conducted research at the Research and Development Center of Samsung Electronics as a Senior Engineer, from 2008 to 2012. From 2012 to 2013, he was with the Brain Korea 21 Information Technology, SNU, as a Postdoctoral Fellow. He conducted research at the Electrical Energy Conversion System Research Division, Korea Electrical Engineering & Science Research Institute, as a Researcher, in 2013. From 2013 to 2016, he worked with the Brain Korea 21 Plus, SNU, as a BK Assistant Professor. In 2014, he was with the University of Bath, Bath, U.K. He is currently an Associate Professor with the School of Electrical and Electronics Engineering, Chung-Ang University, Seoul. His research interests include the analysis and optimal design of next-generation electrical machines using smart materials, such as electromagnet, piezoelectric, and magnetic shape memory alloy.